Characterisation and modelling of the flow behaviour of a medium manganese steel for hot forming

Philipp Althaus[1*], *Radhakanta* Rana[2], *Hendrik* Wester[1], *Johanna* Uhe[1], and *Bernd-Arno* Behrens[1]

[1]Leibniz University Hannover, Institute of Forming Technology and Machines, 30823 Garbsen, Germany
[2]Tata Steel, 1970 CA IJmuiden, Netherlands

Abstract. Medium manganese steels offer a wide range of advantages in hot forming compared to conventional boron steels such as lower heating temperatures and critical quenching rates. Furthermore, the combination of increased strength and ductility makes them a promising material for lightweight components in the mobility sector. For an efficient process design of such components, the finite element simulation is an effective tool to identify a suitable process window and minimise experimental trial-and-error tests. However, a realistic modelling of the material behaviour is essential for reliable simulation results. Therefore, this research focuses on the characterisation and modelling of the flow behaviour of a novel medium manganese steel for the simulation of hot forming processes. Isothermal tensile tests are carried out in a forming and quenching dilatometer under varying forming temperatures and strain rates. To reproduce the heat treatment at the steel producer and the hot forming at the parts manufacturer, the specimens are heat-treated before forming in a process route consisting of annealing, cooling and reheating. After the tests, flow curves are evaluated and modelled using different hardening laws, which are verified by means of numerical simulations.

Keywords: Medium Manganese Steel; Hot Forming; Characterisation; Flow Behaviour.

1 Introduction

In the automotive sector, requirements regarding passenger safety, CO_2 emissions and fuel consumption have steadily increased. In addition, more comfort-relevant components are being integrated into new vehicles. In order to fulfil these demands of safe, comfortable and environmentally sustainable transportation, lightweight construction continues to play a crucial role in the automotive industry [1, 2]. An established process for manufacturing lightweight components with high strength is hot forming [2, 3]. In hot forming, a sheet metal is heated in large roller hearth furnace, transferred to a press and formed with water-cooled stamping tools, whereby rapid quenching is achieved. Due to the high quenching rate, a completely martensitic microstructure is present after forming, which leads to very high strengths with low ductility. For this reason, hot forming is mainly used to produce safety-relevant components, such as A-, B- and C-pillars, bumpers or cross beams [2, 4].

In the automotive industry, the use of boron steels such as 22MnB5 has been established for safety-relevant components, which are heated to approx. 950 °C before forming to achieve austenitisation [5]. However, current developments focus on the improvement of the efficiency of the manufacturing processes as well as the mechanical properties of the steels. In this context, medium manganese steels are increasingly investigated for the potential use in hot forming [6–9]. Medium Mn steels are characterised by a manganese content of 3 to 12 mass % [10–13]. They belong to the third generation of advanced high strength steels (3G-AHSS) and offer an excellent combination of strength and ductility due to the transformation induced plasticity (TRIP) effect [14]. The microstructure of medium Mn steels consists of ferrite, martensite and retained austenite (RA), which is present in a metastable condition. During forming, the RA is transformed into martensite, which results in high strains and increased work hardening, thus leading to a delayed necking. Beside their mechanical properties, medium Mn steels offer advantages in processing. In comparison to conventional boron steels, they can be subjected to lower reheating temperatures [7–9, 15] and lower critical cooling rates [16], which enables energy saving in production. Besides the high strength-ductility ratio, medium Mn steels offer excellent wear resistance, which qualifies them for other industries besides hot forming, e.g. mining machinery [17].

While hot forming of the established boron steels is state-of-the-art and has been investigated by numerous researchers, medium Mn steels are still in the early stage of development. Recent studies focus on the alloy composition and the determination of optimal processing parameters and properties during and after forming. Bilir et al. investigated the thermo-mechanical behaviour of a new medium Mn steel and modelled a hot

* Corresponding author: althaus@ifum.uni-hannover.de

stamping process with the finite element (FE) software PAM-STAMP [18]. It was found that in comparison to 22MnB5, the medium Mn steel was not affected by changes in the transfer or quenching time due to a higher hardenability. As a result, the cost of tool making can be reduced due to lower cooling requirements and more complex parts with higher sheet thicknesses can be produced. Zheng et al. [19] also compared the material properties and formability of a newly developed medium Mn steel with 22MnB5 by means of deep drawing experiments and simulations. It was concluded that the medium Mn steel has a better formability due to a more compact and uniform martensitic structure and thickness distribution after hot forming.

Numerous authors utilise the finite element method (FEM) as an efficient tool to reduce time and costs of process design and enable a deeper understanding of underlaying mechanisms. However, detailed knowledge of the material properties is essential to achieve reliable simulation results. The flow curve is one main input parameter for the modelling of the material behaviour during forming. It defines the onset of plastic deformation and the work hardening of the material. In hot forming, the plastic deformation occurs simultaneously during quenching in the die. Therefore, the characterisation of flow curves should be carried out at different process-relevant temperatures and strain rates [20]. Tong et al. analysed the flow behaviour of a medium Mn steel with 8 wt% Mn under hot stamping conditions using uniaxial tensile tests [21]. An increase of the forming temperature led to a strong reduction of true stress, whereas an increase in strain rate led to a moderate increase of true stress. The total elongation turned out to be insensitive to different forming temperatures and strain rates. In this paper, the flow behaviour of a novel medium Mn steel with a Mn content near to the lower bound for these steels is characterised and modelled under process-relevant conditions for the simulation of hot forming.

2 Methods and procedures

In this study, the medium Mn steel sheets were in uncoated cold rolled condition with a dimension of 1000 mm x 100 mm and a thickness of 1.5 mm. Isothermal tensile tests were carried out to obtain flow curves in the hot forming-relevant process range. For this purpose, the quenching and forming dilatometer DIL 805A/D/T from TA Instruments was used. The test setup and the specimen geometry are shown in Fig. 1.

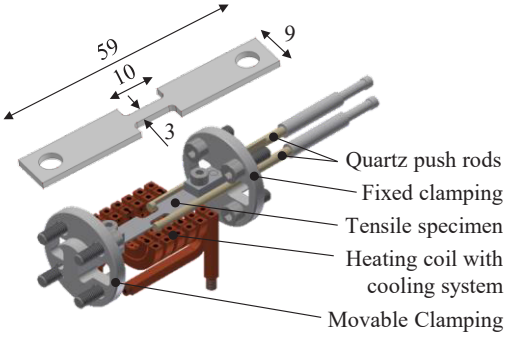

Fig. 1. Test setup and specimen geometry (in mm) [22].

The applicability of the experimental setup with the current specimen geometry for the determination of flow curves was analysed in a former publication [23]. It was found that very good agreement was achieved in comparison to standardised tensile tests according to DIN EN ISO 6892-2. The specimens were taken at 0° to the rolling direction using water jet cutting. For testing, the specimens were clamped between a rigid and a movable holder and heated inductively using a heating coil. The temperature was measured and controlled using a type K thermocouple, which was welded onto the surface of the specimen. To reproduce the industrial process route, the heat-treatment consisted of annealing, cooling, reheating, forming and quenching. Annealing of the cold rolled sheets simulates the last process step at the steel manufacturer, whereas reheating, forming and quenching are used to simulate hot forming process at the parts manufacturer. The times and temperatures of annealing and reheating were determined in a pre-study to find a suitable combination of resulting strength and ductility. With the temperature profile shown in Fig. 2, an ultimate tensile strength of approx. 1150 MPa and total elongations of 15 – 17 % were achieved.

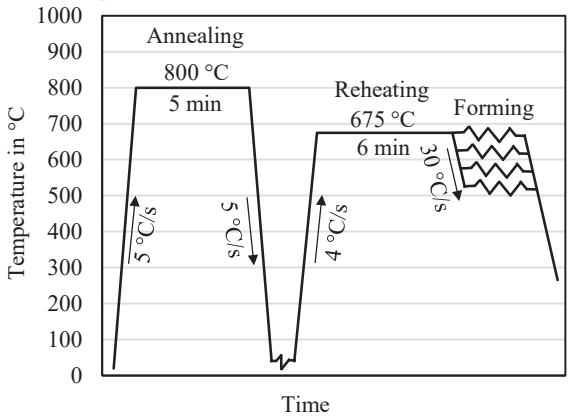

Fig. 2. Heat treatment route consisting of annealing, cooling, reheating and quenching.

The tensile specimens were heated with 5 °C/s to an annealing temperature of 800 °C and held for 5 min. This was followed by cooling with 5 °C/s to room temperature using helium. After a dwell time of 10 min at room temperature, the specimens were heated with 4 °C/s to the reheating temperature of 675 °C and held for 6 min. Then, the specimens were cooled to the forming temperature using helium. When the forming temperature was reached, the specimens were isothermally tested with a constant strain rate until failure. Four forming temperatures between 525 and 675 °C as well as three strain rates between 0.01 and 1 s^{-1} were investigated. The tests were repeated three times. During the tests, the elongation Δl in the tapered part of the specimen was measured with a resolution of 0.01 µm using two quartz push rods. This data was used to calculate the true stress σ and true plastic strain ε according to Equation 1 and 2 by means of the measured forming force F, instantaneous cross-sectional area A_i and initial length l_0.

$$\sigma = \frac{F}{A_i} \quad (1)$$

$$\varepsilon = ln\left(1 + \frac{\Delta l}{l_o}\right) \quad (2)$$

In industrial forming processes, higher strains are reached than in the tensile test. Therefore, the determined flow curves have to be modelled using a hardening law to enable an extrapolation of the flow curve. For the description of the plastic deformation at elevated temperatures, different phenomenological laws can be found in literature. Hensel and Spittel [24] introduced a constitutive model taking strain hardening and softening, strain rate $\dot{\varepsilon}$ and temperature T into account.

$$\sigma = A e^{m_1 T} \varepsilon^{m_2} \dot{\varepsilon}^{m_3} e^{\frac{m_4}{\varepsilon}} (1+\varepsilon)^{m_5 T} e^{m_6 \varepsilon} \dot{\varepsilon}^{m_7 T} T^{m_8} \quad (3)$$

A and $m_{1\text{-}8}$ are material specific constants that are fitted to experimental flow curves. Tang et al. [25] used the Hensel-Spittel law to model the plastic deformation of 22MnB5 in a hot stamping simulation of a Nakajima test. A good accordance between the fitted flow model and the experimental data proved the reliability of the constitutive law for 22MnB5. Lechler et al. [20] also characterised the material behaviour of 22MnB5 for the simulation of hot forming. For the modelling of the plastic deformation, the constitutive law of Norton-Hoff [26] was used, which is a modification and simplification of the Hensel-Spittel law.

$$\sigma = A e^{\frac{\beta}{T}} \varepsilon^{n} \dot{\varepsilon}^{m} \quad (4)$$

To take the initial yield stress as well as the work hardening and strain rate sensitivity into account, the model was extended by Merklein and Lechler [27].

$$\sigma = A e^{\frac{\beta}{T}} (b+\varepsilon)^{n_0 e^{-c_n (T-T_0)}} \dot{\varepsilon}^{m_0 e^{c_m (T-T_0)}} \quad (5)$$

The parameters A, β, b, n_0, c_n, m_0, c_m represent material specific constants and T_0 indicates the lower temperature limit of the hot stamping process. The applicability of the aforementioned hardening laws has been proven for 22MnB5, but not for medium Mn steels. Therefore, in this study, the Hensel-Spittel and modified Norton-Hoff laws will be fitted to the flow curves of the investigated medium Mn steel to evaluate the applicability for hot forming simulations. The model coefficients are calibrated to the experimental flow curves by reducing the sum of the least squares between the experimental flow stress and the flow stress predicted by the hardening laws.

After modelling, the extrapolated flow curves were imported into a material card in Abaqus. To verify the results, a thermo-mechanical simulation model of the conducted tensile tests was created and the resulting force-displacement curves were compared to the experimental data. The FE model with the applied boundary conditions is shown in Fig. 3.

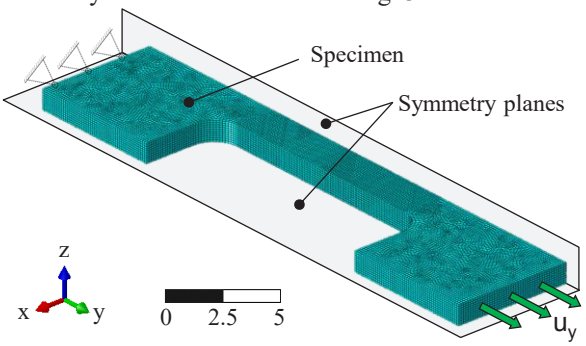

Fig. 3. FE model of the tensile test.

The tensile specimen was meshed with hexahedral elements with a global element length of 0.1 mm and a refined length of 0.075 mm in the examination area. Only one fourth of the specimen was modelled and symmetry boundary conditions were defined to reduce the computational time. One side of the specimen was fixed in accordance to the experiment, whereas a defined displacement was applied to the other side until the maximum measured length change of the experiment was reached. An implicit solver with automatic incrementation was used.

3 Results and discussion

In Fig. 4, the engineering stress-strain diagrams of the isothermal tensile tests are shown for the investigated forming temperatures and strain rates.

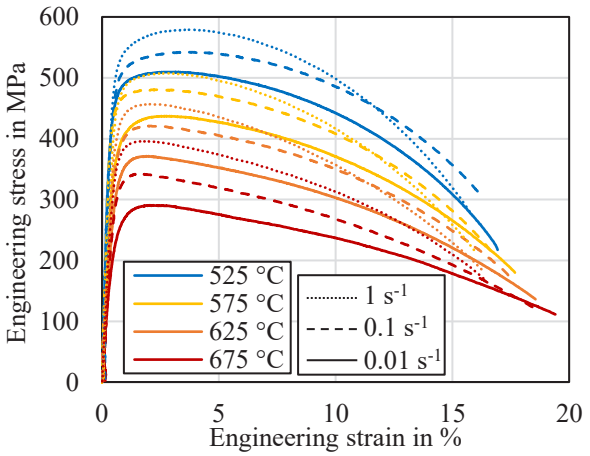

Fig. 4. Engineering stress-strain diagrams for different forming temperatures and strain rates.

With higher forming temperatures, the ultimate tensile strength decreased by 14.5 to 22.1 %, while higher total elongations were reached before material failure. On the contrary, higher strain rates led to a moderate increase of 9.2 to 11.85 % in the tensile strength and lower total elongations before fracture. To model the plastic deformation, flow curves were evaluated by calculating the true stress and true plastic strain according to Equation 1 and 2. The resulting curves are shown in Fig. 5 for the investigated forming temperatures and strain rates.

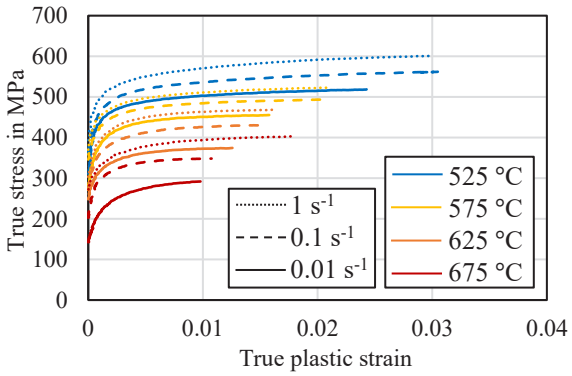

Fig. 5. Flow curves for different forming temperatures and strain rates.

The maximum true plastic strains are very low due to an early onset of necking. After the ultimate tensile strength of the material is reached, the flow curves cannot be evaluated further because a multiaxial stress state is present due to necking. The highest strains are reached at the lowest forming temperature of 525 °C. To enable an extrapolation of the flow curves, the Hensel-Spittel and modified Norton-Hoff hardening laws were fitted to the experimental flow curves. Therefore, the model coefficients were calibrated by reducing the sum of the least squares between the experimental flow stress and the flow stress predicted by the hardening laws. The model parameters are summarised in Table 1.

Table 1. Model coefficients of the hardening laws.

Hensel-Spittel		Mod. Norton-Hoff	
A	5740.70	A	409.13
m_1	-0.00281	β	464.88
m_2	0.00022	b	2.7642E-5
m_3	0.04036	n_0	0.0224
m_4	-0.00028	c_n	-0.00378
m_5	0.00087	m_0	0.00340
m_6	-0.06669	c_m	0.00768
m_7	1.1036E-06		
m_8	0.00029		

To evaluate the prediction accuracies of the hardening laws, Fig. 6 compares the predicted flow curves with the experimental ones at a strain rate of 0.1 s^{-1}.

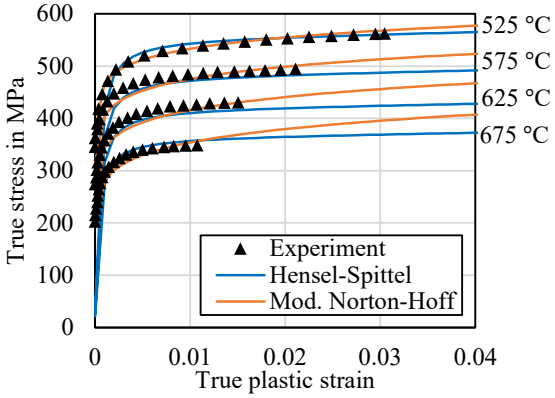

Fig. 6. Comparison of different hardening laws for the modelling of the experimental flow curves.

The modified Norton-Hoff law shows a good prediction of the initial yield stress. Here, the law from Hensel-Spittel shows deviations, because the stress converges against zero for small strains due to the mathematical formulation. Overall, the modified Norton-Hoff law provides a better prediction with a root mean square error (RMSE) of 13.2 MPa compared to the Hensel-Spittel law with a RMSE of 106.9 MPa. For higher strains, the Hensel-Spittel law shows a stronger strain hardening behaviour compared to the modified Norton-Hoff law, which is shown in Fig. 7.

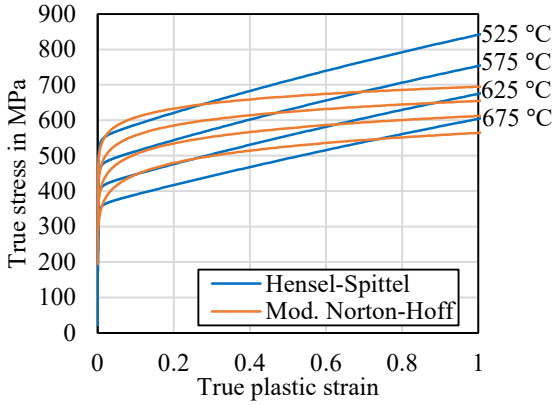

Fig. 7. Predicted flow curves by the hardening laws.

Modified Norton-Hoff law shows a decreasing slope in the flow stress with increasing strains. For further verification, the flow curves were implemented in Abaqus to simulate the tensile tests. In Fig. 8, the experimentally measured force from the tests at 575 °C and a strain rate of 0.1 s^{-1} is compared to the numerical results. Additionally, the error between the simulations and experiment is shown on the secondary axis.

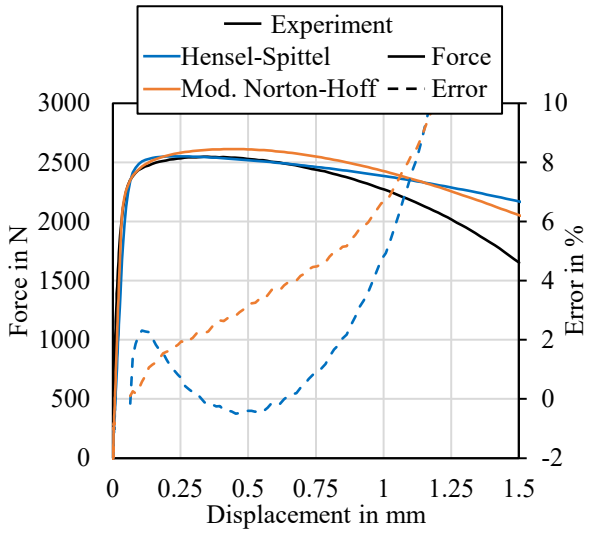

Fig. 8. Comparison of the numerical and experimental force-displacement data and the corresponding error.

Overall, a good prediction accuracy was achieved by both hardening laws up to displacements of approx. 1 mm. The Hensel-Spittel law shows a small overestimation of the forming force at the onset of plastic flow, but provides excellent agreement in the further course, indicated by the small error. The modified law Norton-Hoff shows a good prediction at the onset of plastic deformation, but slightly overestimates the forming force subsequently. After a displacement of 1 mm, both models show increasing errors over 5 %. This can be attributed to the reduction of strength due to the accumulation of damage in the material, which is not taken into account in the simulation. However, both hardening laws show a satisfactory agreement in the region of uniaxial stress and are therefore considered to be verified and can be

used for the simulation of industrial hot forming processes in the future.

Future work should focus on the extension of the experimental flow curves by means of suitable tests which allow higher strains to be reached such as the plane strain compression test. This can improve the prediction accuracy of the hardening laws at higher strains due to a better model calibration. Furthermore, microstructural analyses will be carried out to get a deeper understanding of the phase transformation and distribution as well as the influence on the mechanical properties during and after forming.

4 Conclusions

Hot forming of medium Mn steels offers a high potential for energy savings as they can be formed at lower temperatures compared to conventional boron steels such as 22MnB5 grade. Furthermore, a good combination of strength and ductility can be achieved, which makes them a promising material for lightweight automotive components. The plastic deformation behaviour during forming is mostly influenced by the temperature. An increase in temperature leads to lower flow stresses. Higher strain rates result in a moderate increase of the flow stresses.

For an accurate modelling of the flow behaviour in the hot forming-relevant range, hardening laws need to take strain hardening, strain rate and temperature into account. Established hardening laws that are widely used for 22MnB5 grade were successfully applied for the investigated medium Mn steel and showed a good prediction accuracy in the simulation of the characterisation test.

Acknowledgment

Funded by the Deutsche Forschungsgemeinschaft (DFG, German Research Foundation) - 505217238

References

1. C.A. Romero, P. Correa, E.A. Ariza Echeverri, D. Vergara, Appl. Sci. **14**, 910 (2024)
2. R. Rana, S.B. Singh, Automotive steels: Design, metallurgy, processing and applications (Elsevier/Woodhead Publishing, Amsterdam, Boston, Heidelberg, 2017)
3. B.-A. Behrens, A. Bouguecha, C.M. Gaebel, J. Moritz, J. Schrödter, Procedia Eng. **81**, 1756 (2014)
4. K. Mori, P.F. Bariani, B.-A. Behrens, A. Brosius, S. Bruschi, T. Maeno et al., CIRP Annals **66**, 755 (2017)
5. M. Merklein, M. Wieland, M. Lechner, S. Bruschi, A. Ghiotti, J. Mater. Process. Technol. **228**, 11 (2016)
6. H. Wang, F. Yan, Z. Chang, Steel Res. Int. **95** (2024)
7. R. Rana, T. Kop, P. Beentjes, E. van der Aa, MSF **1105**, 225 (2023)
8. E. van der Aa, R. Rana, Steel Res. Int. **94** (2023)
9. R. Rana, C.H. Carson, J.G. Speer, Hot forming response of medium Mn transformation induced plasticity steels, in *Proceedings of 5th International Conference on Hot Sheet Metal Forming of High-Performance Steel (CHS2 2015), 31 May - 3 June 2015, AIST, Toronto, Ontario, Canada* (2015)
10. W. Ding, N. Zhang, G. Zhang, Y. Li, M. Zhang, J. of Materi Eng and Perform **33**, 2015 (2024)
11. S. Chang, Z. Zhu, X. Huang, J. Zhang, G. Kang, Int. J. Fatigue **181**, 108118 (2024)
12. J. Speer, R. Rana, D. Matlock, A. Glover, G. Thomas, E. de Moor, Metals **9**, 771 (2019)
13. R. Rana, P.J. Gibbs, E. de Moor, J.G. Speer, D.K. Matlock, Steel Res. Int. **86**, 1139 (2015)
14. R. Rana, Mater. Sci. Technol. **35**, 2039 (2019)
15. C. Wang, X. Li, S. Han, L. Zhang, Y. Chang, W. Cao et al., Steel Res. Int. **89** (2018)
16. Y. Chang, C.Y. Wang, K.M. Zhao, H. Dong, J.W. Yan, Mater. Des. **94**, 424 (2016)
17. S. Ge, Q. Wang, J. Wang, Wear **376-377**, 1097 (2017)
18. O.G. Bilir, T. Aycan Başer, A. Karşı, A. Bayram, E. Erişir, Int J Mater Form **15** (2022)
19. G. Zheng, X. Li, Y. Chang, C. Wang, H. Dong, J. of Materi Eng and Perform **27**, 530 (2018)
20. J. Lechler, M. Merklein, M. Geiger, Steel Res. Int. **79**, 98 (2008)
21. C. Tong, Q. Rong, V.A. Yardley, Z. Shi, X. Li, B. Zhang et al., J. Mater. Process. Technol. **306**, 117623 (2022)
22. B.-A. Behrens, D. Rosenbusch, H. Wester, E. Stockburger, J. of Materi Eng and Perform **31**, 825 (2022)
23. B.-A. Behrens, A. Bouguecha, M. Kammler, J. Schrödter, T. Hadifi, T. Götze, Assessment of a Modified Tensile Specimen Geometry for the Characterization of 22MnB5 with a Quenching and Deformation Dilatometer, in *Proceedings of IDDRG 2012, 25-29 November 2012, Bombay, India* (2012)
24. A. Hensel, T. Spittel, Kraft- und Arbeitsbedarf bildsamer Formgebungsverfahren (VEB Deutscher Verlag für Grundstoffindustrie, Leipzig, 1978)
25. B.T. Tang, S. Bruschi, A. Ghiotti, P.F. Bariani, J. Mater. Process. Technol. **228**, 76 (2016)
26. N.J. Hoff, Quart. Appl. Math. **12**, 49 (1954)
27. M. Merklein, J. Lechler, SAE Int. J. Mater. Manf. **1**, 411 (2009)